Research Square

Preprints are preliminary reports that have not undergone peer review.
They should not be considered conclusive, used to inform clinical practice,
or referenced by the media as validated information.

# Pheromone Encapsulation and Release in ZIF-8: Experimental and DFT Insights for Termite Control in Cultural Heritage

**Pi-Chen Wei**
National Ilan University
**Jeng-Shiung Chen**
Yottadeft (Taiwan)
**Tung-Yuan Yung**
National Atomic Research Institute
**Chih-Min Wang**
National Taiwan Ocean University
**Po-Tuan Chen**
chenpotuan@ntut.edu.tw

National Taipei University of Technology

**Article**

**Keywords:** ZIF-8, Metal–organic frameworks, Pheromone delivery, Termite control, Density functional theory, Controlled release.

**Posted Date:** April 1st, 2026

**DOI:** https://doi.org/10.21203/rs.3.rs-9232011/v1

**License:** This work is licensed under a Creative Commons Attribution 4.0 International License. Read Full License

**Additional Declarations:** No competing interests reported.

# Pheromone Encapsulation and Release in ZIF-8: Experimental and DFT Insights for Termite Control in Cultural Heritage

*Pi-Chen Wei [a], Jeng-Shiung Chen [b], Tung-Yuan Yung [c], Chih-Min Wang [d,*], Po-Tuan Chen [e,*]*

[a] Department of Food Science, National Ilan University, Yilan 260, Taiwan, Republic of China. pcwei@niu.edu.tw

[b] Yottadeft Optoelectronics Technology Co., Ltd., Taipei 10460, Taiwan. jsc@yottadeft.com

[c] National Atomic Research Institute, Lungtan, Taoyuan 32546, Taiwan. tyyung@iner.gov.tw

[d] Institute of Bioscience and Biotechnology, National Taiwan Ocean University, Keelung, 202 Taiwan. cmwang@ntou.edu.tw

[e] Department of Vehicle Engineering, National Taipei University of Technology, Taipei 10608, Taiwan. chenpotuan@ntut.edu.tw

**AUTHOR INFORMATION**

Chih-Min Wang: E-mail address: cmwang@ntou.edu.tw. Tel.: +886-2- 2462-2192 ext. 5514.

Po-Tuan Chen: E-mail address: chenpotuan@ntut.edu.tw

**ABSTRACT**

Nanotechnology has steered cultural heritage preservation toward more environmentally friendly and sustainable practices. In this study, pheromones and metal–organic frameworks (MOFs) were integrated to achieve selective pest control. In accordance with the principles of green chemistry, room-temperature aqueous synthesis was performed to prepare a nanoscale MOF called zeolitic imidazolate framework-8 (ZIF-8). A pheromone called *n*-butyl-*n*-butyrate (Drug b) was then integrated with ZIF-8 to achieve termite control through its sustained release. The synthetic process was then systematically modified to achieve suitable synthesis conditions. X-ray diffraction, dynamic light scattering, scanning electron microscopy, and thermogravimetric analysis were performed to confirm the synthesis of nanoscale ZIF-8. The results indicated that the products had a particle size of approximately 134 nm. Drug b was successfully loaded into ZIF-8 and released in a sustained manner. In accordance with density functional theory, the force binding Drug b with ZIF-8 was slightly greater than that binding Drug b with the solvent. Therefore, the loading of Drug b required proper stirring. However, the force binding Drug b with ZIF-8 was not excessively strong to the point of impeding the evaporation of Drug b. These findings confirmed that MOFs can be effectively used to overcome challenges in cultural heritage preservation, a new field of application for this novel material.

**KEYWORD**:
ZIF-8; Metal–organic frameworks; Pheromone delivery; Termite control; Density functional theory; Controlled release.

## I. Introduction

Nanomaterials offer greater versatility and functional diversity than conventional materials, enabling their use in a wide range of emerging applications. In recent years, porous nanomaterials have attracted increasing attention for applications in cultural heritage preservation. Among porous materials, zeolite has long been widely employed because of its stable framework and adsorption capability. Building on the concept of zeolite-based porous structures, other advanced porous materials—most notably metal–organic frameworks (MOFs)—have been developed by incorporating additional metal ions and organic linkers or by adjusting their compositional elements [1,2]. Owing to their exceptionally high specific surface area and tunable pore structures, MOFs have been extensively investigated for applications such as gas storage, gas separation, and drug delivery systems [3,4,5,6,7]. For example, Dedecker et al. demonstrated that MOFs can effectively adsorb acetic acid, a common gaseous pollutant found in museum environments [8]. By exploiting the selective adsorption properties of the porous framework, the MOFs were able to capture acetic acid, which is known to cause aggregation of cellulose fibrils in paper artifacts, corrosion of metallic objects, and deterioration of limestone materials. Compared with conventional adsorbents such as activated carbon and zeolite, MOFs exhibited superior adsorption performance for this application [9]. In another development, the Centre National de la Recherche Scientifique in France fabricated MOF-based paper membranes capable of adsorbing organic solvents present in the environment, and the innovation was subsequently patented [10]. These studies highlight how the growing need for cultural heritage conservation has stimulated the advancement of nanomaterials research.

MOFs are crystalline porous materials constructed from metal nodes and organic ligands connected through coordination bonds. Their modular nature allows the formation of diverse structures through self-assembly, and new MOF architectures can be generated by modifying the organic linkers attached to the metal centers [11]. Among the many subclasses of MOFs, zeolitic imidazolate frameworks (ZIFs) possess a topology analogous to that of zeolites. ZIF structures typically consist of tetrahedrally coordinated transition-metal ions bridged by imidazolate ligands, with zinc and cobalt being the most commonly used metal centers. As porous crystalline materials with zeolite-like structures, ZIFs combine the advantages of both zeolites and MOFs [12]. Because of their high surface area and adjustable pore sizes, ZIF materials have been widely studied for applications including catalysis, molecular separation, gas storage, sensing, and drug delivery [13,14,15,16,17]. Among them, zeolitic imidazolate framework-8 (ZIF-8) is one of the most extensively investigated members of the ZIF family. ZIF-8 can be synthesized by mixing zinc ions with the organic ligand 2-methylimidazole in a solvent under mild conditions, typically through simple stirring at room temperature [18]. The resulting framework consists of tetrahedral Zn–N coordination units that form a highly porous

network. Due to its excellent chemical and thermal stability, high porosity, and extremely large surface area, ZIF-8 has been widely explored for applications such as gas adsorption, catalysis, and sensing. Moreover, the properties and structures of ZIF-8 can vary depending on the synthesis conditions. For instance, the choice of solvent (e.g., water, ethanol, methanol, or dimethylformamide) or imidazole ligand (e.g., 2-methylimidazole or benzimidazole derivatives) can influence the resulting framework structure and physicochemical properties [19]. Similarly, processing parameters such as precursor concentration, solvent environment, synthesis temperature, and the addition of surfactants or alkaline agents can significantly affect the morphology and particle size of ZIF-8 crystals [20]. Consequently, by carefully adjusting these parameters, ZIF-8 materials can be engineered for specific functional applications.

In the context of cultural heritage preservation, protecting wooden artifacts and paintings from termite damage remains an important challenge. Termites can severely deteriorate wooden cultural relics; therefore, effective control strategies are necessary. Matsuura et al. reported that certain pheromone compounds can be used to regulate termite populations. In particular, n-butyl-n-butyrate (hereafter referred to as Drug b) and 2-methyl-1-butanol (Drug m) were found to significantly suppress the reproductive activity of female neotenic termites [21]. Compared with conventional chemical preservatives, pheromone-based approaches offer several advantages. For instance, unlike copper oxide released from alkaline copper quaternary (ACQ) wood preservatives, pheromones can selectively target specific insect species without causing unintended harm to non-target organisms.

Despite these advantages, studies investigating the use of systematically designed porous nanomaterials as carriers for pheromone storage and controlled release remain limited. In particular, the molecular-level interactions governing the adsorption, retention, and release of pheromone molecules within porous frameworks have not been fully clarified. Therefore, in the present study, the highly stable porous material ZIF-8 was combined with Drug b to evaluate its potential as a carrier for pheromone delivery. Various synthesis and loading conditions were investigated to identify the optimal configuration of the ZIF-8 material. The experimental results confirmed that ZIF-8 loaded with Drug b can effectively inhibit termite activity, suggesting its potential application in protecting wooden cultural heritage materials. To further understand the adsorption mechanism, density functional theory (DFT) calculations were performed. The results indicated that Drug b can enter the pores of ZIF-8 only when the interaction strength between Drug b and the ZIF-8 framework exceeds that between Drug b and the surrounding solvent molecules. Conversely, when the interaction between Drug b and ZIF-8 becomes comparable to the intermolecular forces among Drug b molecules, the pheromone can be gradually released into the environment rather than remaining permanently bound to the carrier. To characterize the synthesized materials, X-ray diffraction (XRD), scanning electron microscopy (SEM), and dynamic light scattering (DLS) were employed to analyze their crystal structure, surface morphology, and particle size distribution, respectively.

In addition, thermogravimetric analysis (TGA) was conducted to evaluate the drug-loading capacity of the prepared ZIF-8 materials.

## II. Methods

### *2.1. Calculation Method*

To explain that Drug b can be stored in and released from ZIF-8, we used density functional theory (DFT) to evaluate the adsorption energy of Drug b with ZIF-8 models and solvent molecules. The ZIF-8 model is to binding four 2-methylimidazoles to Zn center and then terminating N of 2-methylimidazoles with additional Zn atoms. The solvent molecules were $H_2O$ and $CH_3OH$. The C, H, N, and O, atom in ZIF-8 models and solvent molecules were calculated with the LANL2DZ basis set [22]. The geometry optimization was performed. All complexes were fully characterized as minima by frequency analysis and evaluated for their zero-point energies (ZPE). The DFT calculations were performed with Gaussian 16 [23].

The drug molecules preferred to be adsorbed near Zn sites of ZIF-8. However, the experimental MOF has a small proportion of Zn site exposure, thus we controlled the adsorption of drug molecules near $CH_3$ groups and penta-cyclic rings of 2-methylimidazole. The interaction energy ($E_{ads}$) is defined as the difference between the energy of the binary system (X-Y) and the sum of the energies of all molecules. For example, the interaction energy between Drug b and ZIF-8 can be formulated as follows:

$$E_{ads} = E(\text{Drug b-ZIF-8}) - [E(\text{Drug b}) + E(\text{ZIF-8})]. \quad (1)$$

### *2.2. Experiment*

Nanomaterials can be synthesized using a variety of methods, such as high-temperature solid-state synthesis, flux growth, chemical transport, intercalation, hydrothermal reactions [24], solvothermal synthesis, room-temperature aqueous synthesis, microwave synthesis, steam-assisted conversion, ultrasonic synthesis [25,26], electrochemical synthesis [27], mechanochemical reactions, and reverse microemulsion. Because the desired crystalline size and synthesis time can be achieved by selecting a suitable synthesis method, the most suitable method for a given application depends on the desired material properties.

This study selected room-temperature aqueous synthesis as the synthesis method. In room-temperature aqueous synthesis, an aqueous solution is used as the reaction medium. Metal and chemical substances are added to this aqueous solution and allowed to react at room temperature. This synthesis method is widely used because of its simplicity, relative swiftness, and energy efficiency. The primary objective of this experiment was to synthesize nanoscale ZIF-8 and evaluate their drug-carrying capacities. All processes conducted in the experiment conformed to the standards of green chemistry, including zero molecular-level environmental pollution, reduction of pollution through source reduction, and absence of hazardous products. The experiment was designed to produce minimal amounts of methanol and liquid waste. The

practicality of the experimental processes was also considered, and the steps and equipment used in the experiment were designed with simplicity, safety, and cost-effectiveness considerations.

(1) Synthesis of ZIF-8

Various molar ratios of raw materials were used to synthesize ZIF-8. The raw materials were $Zn(NO_3)_2 \cdot 6H_2O$ (zinc nitrate hexahydrate, hereinafter referred to as Zn) and 2-methylimidazole (hereinafter referred to as Hmim). The molar ratio of these two raw materials is expressed as Hmim/Zn. Five molar ratios were used in the experiment:

Hmim/Zn = X, X = 1, 2, 4, 8, and 16.

The procedure was as follows: Hmim was first dissolved in 50 mL of methanol (MeOH), and then Zn was slowly added to the methanol solution and stirred for 12 h at room temperature. Subsequently, the solution was centrifuged at 800 rpm for 30 min. The product, ZIF-8, was then collected, rinsed several times with methanol, and baked dry. The aforementioned molar ratios were used. The products are expressed as ZIF-8-XM according to the molar ratio (X) at which they were synthesized.

(2) Drug loading onto ZIFs

Drug loading experiments were conducted using three different procedures to examine the effect of the mixing sequence between ZIF-8, solvent, and Drug b.

In the first method, ZIF-8 was first dispersed in 25 mL of water. Drug b (0.6934 mmol) was then added, and the mixture was stirred for 15, 30, 60, and 120 min. After stirring, the suspension was centrifuged at 8000 rpm, rinsed several times with water to remove unbound molecules, and the collected product was denoted as Z+H+b-XM, where X represents the molar ratio.

In the second method, Drug b (0.6934 mmol) was first mixed with ZIF-8 before adding the mixture into 25 mL of water. The suspension was stirred for 15, 30, 60, and 120 min, followed by centrifugation at 8000 rpm. The solid product was washed several times with water and labeled as Z+b+H-XM.

In the third method, ZIF-8 was first dispersed in 25 mL of methanol. Drug b (0.4394 mmol) was then added, and the mixture was stirred for 12 h. After centrifugation at 8000 rpm, the collected solid was washed several times with methanol and denoted as Z+b-XM.

(3) Drug release test

Add drug-loaded ZIF-8 to water, stir, and record the amount of released drug.

## III. Results and Discussion

### *3.1. Adsorption energy calculations*

Figure 1 provides a detailed comparison of the intermolecular interactions between the two drug molecules (Drug m and Drug b), common solvent molecules ($H_2O$ and $CH_3OH$), and

the ZIF-8 framework based on DFT calculations. These results offer insights into the competitive adsorption behavior that determines whether a drug molecule can be effectively encapsulated inside the pores of the ZIF-8 structure.

As illustrated in Figure 1(a), Drug m forms hydrogen-bonding interactions with both $H_2O$ and methanol molecules. The optimized structures show that the hydrogen-bond distance between Drug m and $H_2O$ is approximately 1.76 Å, while the corresponding distance between Drug m and methanol is slightly shorter at 1.75 Å. These short intermolecular distances indicate relatively strong hydrogen-bonding interactions between Drug m and the surrounding solvent molecules. The calculated adsorption energies further support this observation. The interaction energy between Drug m and $H_2O$ is −6.87 kcal/mol, and that between Drug m and $CH_3OH$ is −7.27 kcal/mol. These values indicate that Drug m has a strong thermodynamic preference for interacting with solvent molecules through hydrogen bonding. In contrast, the interaction between Drug m and the ZIF-8 model is considerably weaker. The calculated adsorption energy of Drug m on the ZIF-8 framework is only −4.23 kcal/mol, which is significantly less negative than the interaction energies with the solvent molecules. Although the optimized structure shows that Drug m approaches the ZIF-8 model at a distance of approximately 2.27 Å, the relatively weak adsorption energy indicates that the interaction is dominated mainly by weak van der Waals forces rather than strong hydrogen bonding or coordination interactions. Because the solvent–drug interaction is thermodynamically more favorable than the drug–MOF interaction, Drug m tends to remain solvated in the solution rather than being adsorbed onto or inserted into the ZIF-8 pores. Therefore, under typical room-temperature conditions, the probability of successfully loading Drug m into the ZIF-8 framework is expected to be relatively low. The solvent molecules effectively compete with the ZIF-8 adsorption sites, stabilizing Drug m in the liquid phase.

A distinctly different behavior is observed for Drug b, as presented in Figure 1(b). Similar to Drug m, Drug b also forms hydrogen bonds with solvent molecules. The calculated intermolecular distances are 1.80 Å for the Drug b–$H_2O$ interaction and 1.82 Å for the Drug b–methanol interaction, indicating typical hydrogen-bond strengths comparable to those observed for Drug m. The adsorption energies are −6.72 kcal/mol with $H_2O$ and −6.80 kcal/mol with $CH_3OH$, respectively. These values suggest that Drug b also interacts favorably with solvent molecules in solution. The key difference arises in the interaction between Drug b and the ZIF-8 framework. The calculated adsorption energy of Drug b with ZIF-8 reaches −8.35 kcal/mol, which is significantly more negative than the interaction energies with the solvent molecules. Despite the optimized Drug b–ZIF-8 distance being slightly longer (2.15 Å) than the hydrogen-bond distances with the solvents, the stronger adsorption energy indicates that the interaction with the ZIF-8 framework is thermodynamically more stable. This stronger binding may originate from multiple cooperative interactions, including van der Waals forces, possible electrostatic interactions, and favorable geometric matching between Drug b and the pore

environment of ZIF-8.

Because the drug–MOF interaction energy for Drug b exceeds the drug–solvent interaction energies, Drug b is more likely to displace solvent molecules and bind to the internal surface of the ZIF-8 pores. Consequently, under sufficient mixing or stirring conditions, Drug b can gradually diffuse into and be stabilized within the ZIF-8 framework. This energetic preference explains why Drug b can be effectively loaded into the porous structure of ZIF-8, while Drug m remains predominantly solvated in the surrounding medium. The DFT results demonstrate that the competition between solvent–drug and MOF–drug interactions plays a critical role in determining drug loading efficiency. The stronger adsorption energy of Drug b with ZIF-8 compared to solvent interactions provides the thermodynamic driving force for encapsulation, whereas the weaker ZIF-8 interaction observed for Drug m limits its incorporation into the MOF pores. These findings highlight the importance of molecular structure and interaction strength in designing efficient MOF-based drug delivery systems.

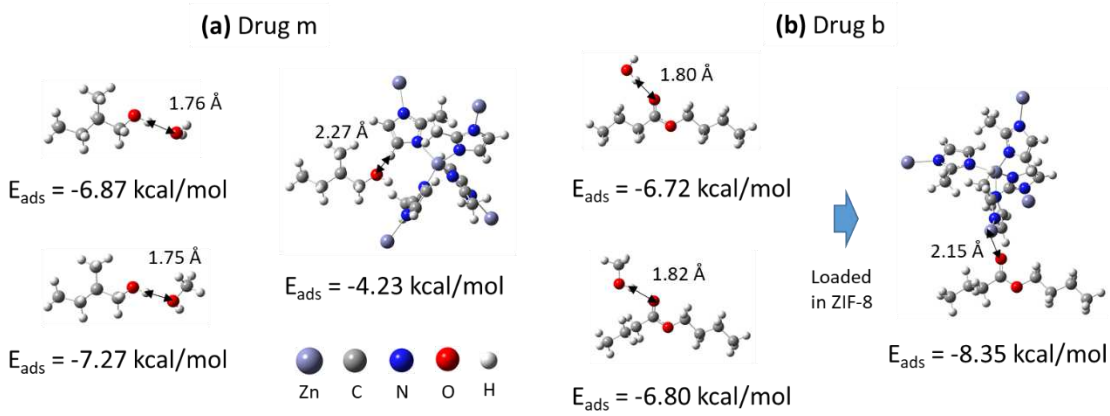



**Figure 1.** DFT calculation of the binding interaction of (a) Drug m and (b) Drug b with solvent and ZIF-8 model.

*3.2. Structural analysis of ZIF-8*

To analyze the structures of the materials, X-ray diffraction (XRD) measurements were performed. As shown in Figure 2(a), numerous characteristic diffraction peaks corresponding to the ZIF-8 structure were observed, including the (011), (002), (112), (022), (013), (222), (114), (233), (134), and (044) planes. The positions and relative intensities of these peaks are consistent with those reported in previous studies [28], confirming the successful formation of the ZIF-8 crystalline framework. Notably, all diffraction peaks display an extremely narrow full width at half maximum, indicating that the synthesized materials possess high crystallinity. Furthermore, the XRD patterns of ZIF-8 loaded with Drug m and Drug b remain nearly identical to that of pristine ZIF-8, suggesting that the adsorption of drug molecules does not significantly alter the crystal structure or long-range ordering of the framework.

SEM was employed to examine the surface morphology of the synthesized materials, as

shown in Figure 2(b) and 2(c). The images reveal that the ZIF-8 particles exhibit well-defined polyhedral shapes with clear crystal facets, indicating good crystallinity and structural integrity. These morphological features are consistent with the XRD results, confirming that the ZIF-8 framework remains stable even after drug adsorption. Specifically, SEM observations were performed for ZIF-8-8M (Figure 2(b)) and ZIF-8-2M (Figure 2(c)). The particle size distribution of ZIF-8-8M appears relatively uniform, whereas ZIF-8-2M shows a broader size distribution with some larger particles (indicated by black arrows). Using ImageJ software, the average particle size of ZIF-8-8M was estimated to be approximately 300 nm, which is close to the value obtained from the DLS analysis. In contrast, the DLS results for ZIF-8-2M indicate a much wider particle size distribution, with an upper size limit of approximately 2000 nm, which agrees with the presence of larger particles observed in the SEM images. Because the SEM images represent a relatively small observation area (7000 × 4730 $nm^2$), the difference between the local microscopic SEM observations and the macroscopic DLS measurements is reasonable, particularly for samples such as ZIF-8-2M with broad particle size distributions.

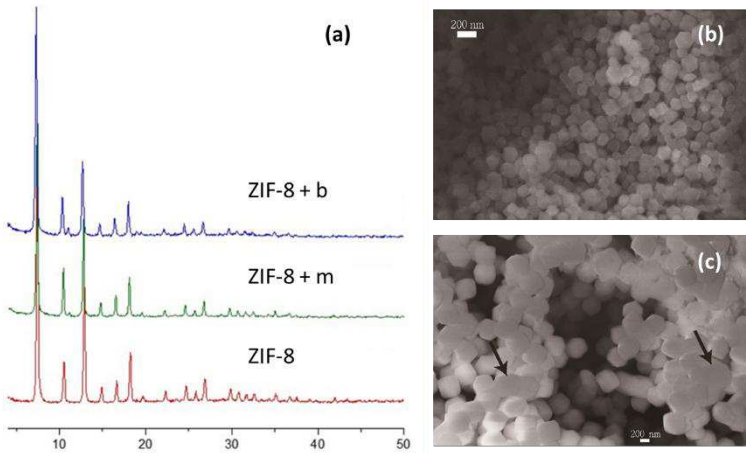



**Figure 2.** XRD characterizations of (a) ZIF-8 and ZIF-8 with drug loading. SEM images of ZIF-8 with Hmim/Zn molar ratios: (b) ZIF-8-8M and (c) ZIF-8-2M.

In this study, five products were synthesized using the aforementioned methods with Hmim/Zn molar ratios of 1, 2, 4, 8, and 16. DLS was employed to analyze the particle sizes of the products. DLS provides several advantages, including the ability to measure particle size distributions in relatively large liquid samples (on the scale of several milliliters). Because the technique is optical and nondestructive, it allows particle size characterization at room temperature and enables a comprehensive evaluation of the size distribution. The particle sizes of ZIF-8 synthesized at different molar ratios are summarized in Table 1. The measured particle sizes were 347.2 nm for ZIF-8-1M, 2004.3 nm for ZIF-8-2M, 1095.7 nm for ZIF-8-4M, 296.2 nm for ZIF-8-8M, and 310.7 nm for ZIF-8-16M. Among these samples, the smallest particles were obtained at a molar ratio of 8 (ZIF-8-8M), whereas the largest particles were formed at a

molar ratio of 2 (ZIF-8-2M). Specifically, the particle size of ZIF-8-8M was 296.2 nm, while that of ZIF-8-2M reached 2004.3 nm. Therefore, subsequent analyses focused on ZIF-8-2M and ZIF-8-8M, representing the samples with the largest and smallest particle sizes, respectively, to evaluate the influence of particle size on drug loading performance.

Table 1. Average particle sizes of ZIF-8 with Hmim/Zn molar ratios of 1, 2, 4, 8, and 16.

| | ZIF-8-1M | ZIF-8-2M | ZIF-8-4M | ZIF-8-8M | ZIF-8-16M |
|---|---|---|---|---|---|
| Particle size (nm) | 347.2 nm | 2004.3 | 1095.7 | 296.2 | 310.7 |

*3.3. Drug-carrying capacities of ZIF-8*

In this study, TGA was conducted to evaluate the drug-carrying capacities of the samples. TGA is commonly used to examine how temperature influences the weight of a material and can also reveal whether organic components in a sample undergo evaporation or thermal decomposition upon heating, leaving behind inorganic residues. Because TGA monitors the response of a sample to temperature changes through variations in weight, the distinct boiling points of different substances can be used to determine whether a drug has been successfully loaded into the material. ZIF-8-8M was selected for the drug-loading experiments. To evaluate the interaction between Drug b and ZIF-8, Drug m (1.1344 mmol) was prepared under the same conditions and used as a control sample. The corresponding TGA curves for ZIF-8-8M loaded with Drug m and Drug b are shown in Figure 3(a) and Figure 3(b), respectively. Drug m and Drug b exhibit evaporation-induced weight loss at their boiling points, approximately 130°C and 164–165°C, respectively. These characteristic temperatures can therefore be used to estimate the amount of drug incorporated into the ZIF-8 framework.

As shown in Figure 3(a), Drug m was not effectively loaded into ZIF-8. The TGA curves show a continuous decrease in weight with increasing temperature regardless of whether the drug was added to ZIF-8 first or ZIF-8 was added to water first, indicating that Drug m was not retained within the framework. In contrast, the TGA curves in Figure 3(b) reveal a different behavior for Drug b. Regardless of whether Drug b was added to ZIF-8 first or ZIF-8 was dispersed in water first, no obvious weight change is observed between 200°C and 300°C, suggesting that only a small amount of loosely bound drug evaporated in this temperature range. However, at approximately 300°C, a total weight difference of about 20% compared with the initial state is observed, which can be attributed to the decomposition of Drug b loaded within the ZIF-8 structure. The difference between the two preparation routes—Drug added to ZIF-8 first (ZbH-8M) and ZIF-8 added to water first (ZHb-8M)—is relatively small, with only about a 1% weight difference at 300°C. Notably, the second degradation temperature of ZHb-8M is approximately 40°C higher than that of ZbH-8M, indicating that ZHb-8M exhibits slightly higher thermal stability. This higher stability suggests a broader temperature range for the

release of Drug b from the ZIF-8 framework.

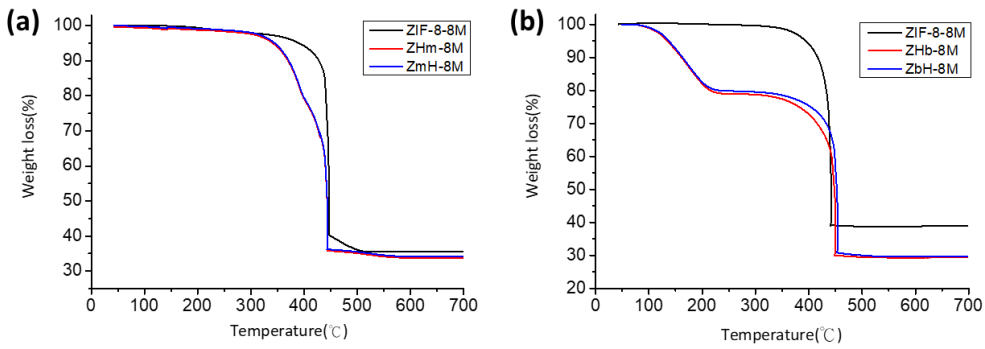



Figure 3. TGA curves of ZIF-8-8M loaded with (a) Drug m and (b) Drug b (the black curve represents unloaded ZIF-8).

*3.4. Drug loading analysis of ZIF-8*

In this study, the effects of drug loading time were compared between ZHb-2M and ZHb-8M. Both samples were loaded with Drug B by stirring for 15, 30, 60, and 120 min. After stirring, the samples were removed and analyzed using TGA. As displayed in **Error! Reference source not found.**, the weights of both samples considerably differed at 200°C–300°C and at the initial unheated state. Table 2 depicts the weight percentage of the loaded drug, which was inferred from the weight loss. Although molar ratios of 8 and 2 exhibited similar trends, as time passed, ZHb-8M considerably outperformed ZHb-2M. After 15 min, the average weight loss percentages stabilized at 30, 60, and 120 min of stirring, indicating that the drug was loaded into ZIF-8 after 30 min of stirring. This result indicated that an increase in stirring time had a limited effect on the amount of drug loaded.

Table 2. Weight percentage loss of the loaded Drug b in ZIF-8 with Hmim/Zn molar ratios of 2 and 8.

| | 5 min | 15 min | 30 min | 60 min | 120 min |
|---|---|---|---|---|---|
| ZHb-2M | 71.9% | 66.9% | 71.5% | 70.8% | 71.3% |
| ZHb-8M | 72.0% | 69.30% | 72.36% | 72.54% | 72.63% |

After 30, 60, and 120 min of stirring, the average weight loss percentages of the samples were calculated. The results revealed that the values of ZHb-2M and ZHb-8M remained at approximately 22.4% and 23.1%, respectively, indicating that the drug loading performance of ZHb-8M exceeded that of ZHb-2M. Therefore, with consideration of both drug loading performance and stirring time, the ZHb-8M sample that underwent 30 min of stirring (ZHb-8M-30min) was deemed the optimal option.

*3.5. Drug release analysis of ZIF-8*

TGA was used again to perform a drug release analysis. Both ZHb-2M and ZHb-8M were loaded with Drug b by stirring for 30 min. The samples were then dissolved in water; stirred for 5 min, 90 min, 300 min, 2 days, and 3 days; and dried to measure weight loss through TGA. **Error! Reference source not found.**(a) and 4(b) depict the TGA results of ZHb-2M and ZHb-8M at various drug release times. Increasing the stirring time increased the amount of Drug b released into the water, which resulted in a decrease in the amount of drug in ZIF over time. Therefore, evaluating the sample using TGA after drug release revealed the extent to which Drug b remained in the sample. The results indicated that both ZHb-2M and ZHb-8M underwent a considerable weight loss after drug release for a certain period of time. The difference observed in the weight percentage represented the amount of Drug b that remained in the sample. At temperatures between 200°C and 300°C, minor weight changes were observed, indicating the complete exhaustion of Drug b that was loaded into the samples. At nearly 300°C, the samples started to lose weight rapidly, suggesting the rapid disintegration of ZIF-8.

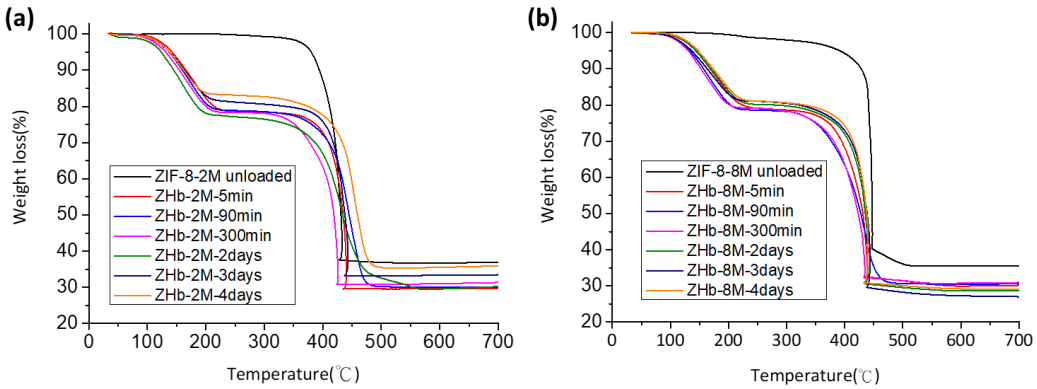



Figure 4. Weight loss percentages of Drug b from (a) ZHb-8M and (b) ZHb-2M at various releasing times measured using TGA.

Table 3 depicts the relationship between the weight loss percentages (drug residue percentages) and drug release times of ZHb-2M and ZHb-8M. Both ZHb-2M and ZHb-8M were loaded with Drug b by stirring for 30 min. Among all samples, the ZHb-2M and ZHb-8M samples that were stirred for 4 days had the lowest weight loss percentages, suggesting that the amount of drug remaining in ZIF-8 decreased as the drug release time increased. However, the ZHb-2M-30min samples that were exposed to drug release for 3 and 4 days had the highest and lowest weight loss percentages, respectively, suggesting unstable drug release performance. These findings may be attributable to the wide particle size distribution of ZHb-2M-30min. Previously, the drug loading performance of ZHb-2M-30min and ZHb-8M-30min was calculated as 22.4% and 23.1%, respectively.

Table 3. Release results of ZIF-8 with Hmim/Zn molar ratios of 2 and 8 after adding Drug b for 5 minutes, 90 minutes, 300 minutes, 2 days, 3 days, and 4 days respectively

| | ZHb-2M | ZHb-8M |
|---|---|---|
| 0 min | 71.52% | 72.36% |
| 5 min | 70.47% | 70.06% |
| 90 min | 69.99% | 69.58% |
| 300 min | 69.18% | 69.32% |
| 2 days | 70.59% | 71.41% |
| 3 days | 66.79% | 73.01% |
| 4 days | 64.7% | 70.97% |

## IV. Conclusion

Growing awareness of sustainable development has redirected cultural heritage preservation toward green and sustainable practices and techniques. To preserve cultural heritage and the local landscape and environment, sustainable, ecofriendly, and rational solutions must be applied. To achieve environmental protection, the application of biotechnology and bioproducts in the preservation of cultural heritage must be based on green chemistry and nanotechnology to align with the goal of environmental protection. In this study, a nanoscale MOF called ZIF-8 was successfully synthesized in various molar ratios using aqueous synthesis, a green chemistry method. According to the XRD analysis results, all five molar ratios (Hmim/Zn) evaluated in this study successfully resulted in the successful synthesis of ZIF-8. According to the SEM and DLS analysis results, when Hmim/Zn = 8, the product ZIF-8-8M had the smallest particle size (111–157 nm, weight mean = 134 nm) and the most uniform particle size distribution, whereas the product ZIF-8-8M had a wider particle size distribution (approximately 700–1000 nm) and the highest particle size weighted mean of 880 nm. The XRD, SEM, and DLS analysis results confirmed the successful synthesis of nanoscale ZIF-8.

During drug loading analysis, two pheromones that inhibit termites were used: *n*-butyl-*n*-butyrate (Drug b) and 2-methyl-1-butanol (Drug m). According to the TGA data, Drug m could not be loaded into ZIF-8, whereas Drug b was successfully loaded. Stirring for 30 min allowed for loading approximately 23% of Drug b. According to the drug release analysis results, compared with ZHb-2M-30min, ZHb-8M-30min released the drug in a steadier and sustained manner. In addition, the crystalline structure of ZIF-8 was suitable for drug loading and release. These findings laid the foundation for developing a natural and environmentally friendly long-acting nanomaterial for cultural heritage preservation. Future studies should focus on carrier structure modification, combination drug application, and loading capacity improvement.

## AUTHOR CONTRIBUTIONS

Pi-Chen Wei: Conceptualization; Investigation; Writing – original draft. Jeng-Shiung Chen: Writing – original draft. Tung-Yuan Yung: Formal analysis. Chih-Min Wang: Conceptualization; Funding acquisition; Supervision. Po-Tuan Chen: Supervision; Funding acquisition; Writing – review & editing.

**ACKNOWLEDGMENTS**

We thank the Computer and Information Network Center at National Taiwan University for providing calculation resources and the financial support provided by the Bureau of Cultural Heritage, Ministry of Culture, Taiwan.

**FUNDING**

Funding support from the National Science and Technology Council (NSTC) in Taiwan (111-2113-M-027-009 and 112-2221-E-027-051-MY3).

**DATA AVAILABILITY**

Data is available from the authors upon reasonable request.

**References**


[1] Dusselier, M., & Davis, M. E. (**2018**). Small-Pore Zeolites: Synthesis and Catalysis. *Chemical Reviews*, *118*(11), 5265–5329.

[2] Rakstys, K., Abate, A., Dar, M. I., Gao, P., Jankauskas, V., Jacopin, G., … Nazeeruddin, M. K. (**2015**). Triazatruxene-Based Hole Transporting Materials for Highly Efficient Perovskite Solar Cells. *Journal of the American Chemical Society*, *137*(51), 16172–16178.

[3] Chakraborty, A., Bhattacharyya, S., Hazra, A., Ghosh, A. C., & Maji, T. K. (**2016**). Post-synthetic metalation in an anionic MOF for efficient catalytic activity and removal of heavy metal ions from aqueous solution. *Chemical Communications*, *52*(13), 2831–2834.

[4] Chandra Rao, P., & Mandal, S. (**2018**). Europium-Based Metal–Organic Framework as a Dual Luminescence Sensor for the Selective Detection of the Phosphate Anion and Fe3+ Ion in Aqueous Media. *Inorganic Chemistry*, *57*(19), 11855–11858.

[5] Lee, J., Farha, O. K., Roberts, J., Scheidt, K. A., Nguyen, S. T., & Hupp, J. T. (**2009**). Metal–organic framework materials as catalysts. *Chemical Society Reviews*, *38*(5), 1450–1459.

[6] Wang, L., Zheng, M., & Xie, Z. (**2018**). Nanoscale metal–organic frameworks for drug delivery: a conventional platform with new promise. *Journal of Materials Chemistry B*, *6*(5), 707–717.

[7] Li, J.-R., Kuppler, R. J., & Zhou, H.-C. (**2009**). Selective gas adsorption and separation in metal–organic frameworks. *Chemical Society Reviews*, *38*(5), 1477–1504.

[8] Kevin Dedecker, Renjith S. Pillai, Farid Nouar, João Pires, Nathalie Steunou, Eddy Dumas, Guillaume Maurin, Christian Serre, and Moisés L. Pinto. Metal-Organic Frameworks for Cultural Heritage Preservation: The Case of Acetic Acid Removal. *ACS Applied Materials & Interfaces* **2018** *10* (16), 13886-13894

[9] Matsuura, K., Himuro, C., Yokoi, T., Yamamoto, Y., Vargo, E. L., & Keller, L. (**2010**). Identification of a pheromone regulating caste differentiation in termites. *Proceedings of the National Academy of Sciences*, *107*(29), 12963–12968.

[10] Biswas, S., Haouas, M., Freitas, C., Soares, C. V., Al Mohtar, A., Saad, A., ... Steunou, N. (**2022**). Engineering of metal–organic frameworks/gelatin hydrogel composites mediated by the coacervation process for the capture of acetic acid. Chemistry of Materials, *34*(21), 9760–9774.

[11] Nam, D., Kim, J., Hwang, E., Nam, J., Jeong, H., Kwon, T.-H., & Choe, W. (**2021**). Multivariate porous platform based on metal-organic polyhedra with controllable functionality assembly. *Matter*, *4*(7), 2460–2473.

[12] Sánchez-Laínez, J., Zornoza, B., Friebe, S., Caro, J., Cao, S., Sabetghadam, A., … Coronas, J. (**2016**). Influence of ZIF-8 particle size in the performance of polybenzimidazole mixed matrix membranes for pre-combustion CO2 capture and its validation through interlaboratory test. *Journal of Membrane Science*, *515*, 45–53.

[13] Bao, Q., Lou, Y., Xing, T., & Chen, J. (**2013**). Rapid synthesis of zeolitic imidazolate framework-8 (ZIF-8) in aqueous solution via microwave irradiation. *Inorganic Chemistry Communications*, *37*, 170–173.

[14] Cravillon, J., Münzer, S., Lohmeier, S.-J., Feldhoff, A., Huber, K., & Wiebcke, M. (**2009**). Rapid Room-Temperature Synthesis and Characterization of Nanocrystals of a Prototypical Zeolitic Imidazolate Framework. *Chemistry of Materials*, *21*(8), 1410–1412.

[15] Keser Demir, N., Topuz, B., Yilmaz, L., & Kalipcilar, H. (**2014**). Synthesis of ZIF-8 from recycled mother liquors. *Microporous and Mesoporous Materials*, *198*, 291–300.

[16] Pan, Y., Liu, Y., Zeng, G., Zhao, L., & Lai, Z. (**2011**). Rapid synthesis of zeolitic imidazolate framework-8 (ZIF-8) nanocrystals in an aqueous system. *Chemical Communications*, *47*(7), 2071–2073.

[17] Şahin, F., Topuz, B., & Kalıpçılar, H. (**2018**). Synthesis of ZIF-7, ZIF-8, ZIF-67 and ZIF-L from recycled mother liquors. *Microporous and Mesoporous Materials*, *261*, 259–267.
[18] Cho, H.-Y., Kim, J., Kim, S.-N., & Ahn, W.-S. (**2013**). High yield 1-L scale synthesis of ZIF-8 via a sonochemical route. *Microporous and Mesoporous Materials*, *169*, 180–184.
[19] Park, K. S., Ni, Z., Côté, A. P., Choi, J. Y., Huang, R., Uribe-Romo, F. J., … Yaghi, O. M. (**2006**). Exceptional chemical and thermal stability of zeolitic imidazolate frameworks. *Proceedings of the National Academy of Sciences*, *103*(27), 10186–10191.
[20] McKinstry, C., Cussen, E. J., Fletcher, A. J., Patwardhan, S. v, & Sefcik, J. (**2013**). Effect of Synthesis Conditions on Formation Pathways of Metal Organic Framework (MOF-5) Crystals. *Crystal Growth & Design*, *13*(12), 5481–5486.
[21] Matsuura, K., Himuro, C., Yokoi, T., Yamamoto, Y., Vargo, E. L., & Keller, L. (**2010**). Identification of a pheromone regulating caste differentiation in termites. *Proceedings of the National Academy of Sciences*, *107*(29), 12963–12968.
[22] Hay, P. J. & Wadt, W. R. Ab initio effective core potentials for molecular calculations. Potentials for K to Au including the outermost core orbitals. *J. Chem. Phys. 82*, 299–310 (**1985**).
[23] Frisch, M. J. et al. Gaussian 16 Rev. C.01. (**2016**).
[24] Zhang, J.-P., Liao, P.-Q., Zhou, H.-L., Lin, R.-B., & Chen, X.-M. (**2014**). Single-crystal X-ray diffraction studies on structural transformations of porous coordination polymers. *Chemical Society Reviews*, *43*(16), 5789–5814.
[25] Bang, J. H., & Suslick, K. S. (**2010**). Applications of Ultrasound to the Synthesis of Nanostructured Materials. *Advanced Materials*, *22*(10), 1039–1059.
[26] Leadbeater, N. E. (**2003**). Book Review: Practical Sonochemistry Power Ultrasound Uses and Applications. 2nd edition. By Timothy J. Mason and Dietmar Peters. *Angewandte Chemie International Edition*, *42*(21), 2333–2334.
[27] Mueller, U., Schubert, M., Teich, F., Puetter, H., Schierle-Arndt, K., & Pastré, J. (**2006**). Metal–organic frameworks—prospective industrial applications. *Journal of Materials Chemistry*, *16*(7), 626–636.
[28] Cravillon, J., Schröder, C. A., Bux, H., Rothkirch, A., Caro, J., & Wiebcke, M. (**2012**). Formate modulated solvothermal synthesis of ZIF-8 investigated using time-resolved in situ X-ray diffraction and scanning electron microscopy. *CrystEngComm*, *14*(2), 492–498.